

Mapping quantal touch using 7 Tesla functional magnetic resonance imaging and single-unit intraneural microstimulation

Sanchez-Panchuelo RM^{1*}, Ackerley R^{2,3*}, Glover PM¹, Bowtell RW¹, Wessberg J², Francis ST^{1§} and McGlone F^{4§}

* These authors contributed equally to this work.

§ These authors contributed equally to this work.

¹Sir Peter Mansfield Imaging Centre, School of Physics and Astronomy, University of Nottingham, Nottingham, NG7 2RD, UK

²Department of Physiology, University of Gothenburg, Göteborg, SE-405 30, Sweden.

³Laboratoire de Neurosciences Intégratives et Adaptatives (UMR 7260), Aix-Marseille Université – CNRS, Marseille, France

⁴School of Natural Sciences and Psychology, Liverpool John Moores University, Liverpool, L3 3AF, UK

Corresponding author: Rosa Sanchez Panchuelo

Email: rosa.panchuelo@nottingham.ac.uk

Key words: touch, microneurography, intraneural microstimulation, peripheral nerves, hand, tactile, fMRI, ultra-high field

1 **Abstract**

2 Using ultra-high field 7 Tesla (7T) functional magnetic resonance imaging (fMRI), we
3 map the cortical and perceptual responses elicited by intraneural microstimulation
4 (INMS) of single mechanoreceptive afferent units in the median nerve, in humans.
5 Activations are compared to those produced by applying vibrotactile stimulation to
6 the unit's receptive field, and unit-type perceptual reports are analyzed. We show that
7 INMS and vibrotactile stimulation engage overlapping areas within the
8 topographically appropriate digit representation in the primary somatosensory cortex.
9 Additional brain regions in bilateral secondary somatosensory cortex, premotor
10 cortex, primary motor cortex, insula and posterior parietal cortex, as well as in
11 contralateral prefrontal cortex are also shown to be activated in response to INMS.
12 The combination of INMS and 7T fMRI opens up an unprecedented opportunity to
13 bridge the gap between first-order mechanoreceptive afferent input codes and their
14 spatial, dynamic and perceptual representations in human cortex.

1 INTRODUCTION

2 The primary somatosensory cortex (S1) has been extensively explored in animal
3 studies where it has been shown that this area displays multiple, fine-grained
4 representations of the body (Paul et al. 1972; Kaas et al. 1979; Favorov et al. 1987).
5 Penfield and Boldrey (Penfield & Boldrey 1937) derived the first maps of the
6 somatotopic human body representation in S1 using electrical stimulation of the
7 cortical surface. Somatosensory research in humans has involved using
8 psychophysical (Klatzky et al. 1985; Gescheider et al. 2002), microneurographic
9 (Vallbo & Johansson 1984; Johansson & Vallbo 1983), and neuroimaging (McGlone
10 et al. 2002; Martuzzi et al. 2014; Servos et al. 2001) techniques to study different
11 stages and levels of detail in somatosensory function. Functional magnetic
12 resonance imaging (fMRI) has been used extensively for non-invasive study of the
13 somatosensory cortices in humans (Nelson & Chen 2008; McGlone et al. 2002;
14 Sanchez-Panchuelo et al. 2010). Most such fMRI studies have investigated the
15 spatial pattern of cortical activation in response to vibrotactile (Francis et al. 2000;
16 Sanchez-Panchuelo et al. 2010) or pneumatic (Huang & Sereno 2007; Overduin &
17 Servos 2008) mechanical stimulation of the digits, or to electrical stimulation of the
18 skin (Blankenburg et al. 2003) or median nerve (Kampe et al. 2000; Ferretti et al.
19 2007). These approaches excite large populations of different classes of
20 mechanoreceptive afferents resulting in relatively diffuse activations in contralateral
21 S1 and bilateral secondary somatosensory cortex (S2).

22 Microneurography provides a method to record the spike discharge activity of
23 a single mechanoreceptive afferent in conscious humans (Vallbo & Hagbarth 1968)
24 to determine its response to skin contact and the properties of its receptive field, i.e.
25 location, size, and shape. In this manner, mechanoreceptive afferents innervating the
26 glabrous skin of the hand can be categorized into one of four types: fast-adapting
27 type 1 (FA1), fast-adapting type 2 (FA2), slowly-adapting type 1 (SA1), and slowly-
28 adapting type 2 (SA2)(Vallbo & Johansson 1984). In intraneural microstimulation

1 (INMS), single mechanoreceptive afferents are selectively activated by passing a
2 small (1-7 μ A) current through the recording microelectrode, thus evoking a quantal
3 sensation in the projected sensory field, which matches the physiological qualities of
4 the recorded mechanoreceptive afferent (Torebjörk et al. 1987). Microstimulation of
5 an FA1 afferent evokes a well-defined, local sensation of 'flutter' or 'buzzing', while
6 microstimulation of an SA1 afferent evokes a sensation of continuous pressure or
7 inward pulling (Vallbo et al. 1984; Ochoa & Torebjörk 1983). Microstimulation of an
8 FA2 afferent evokes a diffuse sensation of vibration over a larger area, whereas
9 microstimulation of an SA2 afferent does not produce a consistent, conscious
10 sensory experience (Vallbo et al. 1984; Ochoa & Torebjörk 1983).

11 It has been shown in a small number of previous studies that INMS of single
12 mechanoreceptive afferents can be combined with noninvasive imaging methods to
13 advance our understanding of the effects of mechanoreceptive afferent activity in
14 somatosensory cortices. For example, INMS of FA1 and SA1 afferents in the median
15 nerve produces frequency-following electroencephalography responses within
16 contralateral S1 (Kelly et al. 1997). The single previous study combining INMS with
17 fMRI (Trulsson et al. 2001), using a 3 T scanner and a surface coil positioned over
18 the parietal lobe contralateral to the site of stimulation, showed that INMS of FA1 and
19 SA1 afferents induced activity in S1 and S2, which overlapped with regions activated
20 by applying mechanical vibration to the relevant units' receptive fields. However, a
21 detailed study of other cortical areas activated by single unit INMS has yet to be
22 performed.

23 Several studies have previously assessed the cortical response to vibrotactile
24 stimulation of the glabrous skin of the human hand, and shown that this evokes a
25 hemodynamic response in multiple primary and secondary cortical areas, including
26 contralateral S1, bilateral S2, primary motor cortex (M1), supplementary motor area
27 (SMA), cingulate cortex, posterior parietal cortex (PPC), and insula cortex (McGlone
28 et al. 2002; Trulsson et al. 2001; Gelnar et al. 1998). Ultra-high field (7T) fMRI has

1 also recently been used in conjunction with vibrotactile stimulation to map individual
2 digit representations and resolve the fine, within-digit organization (base-to-tip), thus
3 revealing functional subdivisions of areas in S1 (Sanchez-Panchuelo et al. 2010;
4 Sanchez-Panchuelo et al. 2012). Compared to lower field measurements, 7T fMRI
5 provides greatly increased sensitivity and blood-oxygenation level dependent (BOLD)
6 signal contrast, coupled with improved intrinsic spatial specificity (Gati et al. 1997).
7 Here, we used 7T fMRI to resolve whole-brain cortical activation patterns evoked by
8 INMS of single mechanoreceptive afferent units in the glabrous skin of the hand, and
9 to assess the precise spatial localization of INMS-evoked BOLD responses in
10 contralateral S1, in comparison to activation due to mechanical vibrotactile
11 stimulation.

12

13 **RESULTS**

14 Recordings were made from 28 mechanoreceptive afferents (17 FA1, 14 SA1, 1 FA2
15 and 1 SA2) in 4 participants during 10 experimental sessions. We focused our study
16 on the cortical response to stimulation of type 1 afferents (FA1 and SA1), as these
17 units are far more numerous in the volar hand than type 2 units (FA2 and SA2)
18 (Vallbo & Johansson 1984). Example recordings from FA1 and SA1 units are shown
19 in Figures 1a and 1b respectively, demonstrating that good quality signals can be
20 recorded from single mechanoreceptive afferents in the environment of a 7T
21 magnetic resonance scanner. INMS of single units produced distinct sensations: FA1
22 stimulation was typically felt as vibration or buzzing, while SA1 stimulation elicited a
23 sensation of pressure or pulling (see Table 1).

24 Due to the technically challenging set-up (e.g. 2 units were lost on moving the
25 participant into the scanner bore) and the nature of the method (e.g. the stimulated
26 unit corresponds to the unit from which recordings were previously made only around
27 50 % of the time (Torebjörk et al. 1987)), INMS was carried out during concurrent
28 fMRI in 11 units (U1-U11) that gave single-point sensations, 6 of which were

1 electrophysiologically-characterized (see Table 1). The receptive field locations for
2 these units are shown in Figure 1c.

3

4 **Cortical responses to single unit INMS and vibrotactile stimulation in S1:** Clear
5 and reproducible BOLD responses were found in somatosensory regions, when
6 INMS was perceived. Occasionally, participants reported that the sensation evoked
7 by the INMS stopped, likely due to a minor dislodgement of the microelectrode. This
8 occurred for U7 where a projected sensation was perceived prior to scanning, but no
9 sensation was felt during the fMRI run. For some units, the sensation was weak (U2,
10 U3; possibly due to difficulty in attending to the stimulus sensation when inside the
11 scanner), or lost during the fMRI run (U5, U6, U8). We compared the location of fMRI
12 responses of all perceived INMS units in contralateral S1 with the digit representation
13 obtained from both vibrotactile stimulation of the microstimulated unit's receptive field
14 and the fMRI somatotopy maps formed from the traveling-wave vibrotactile paradigm
15 (Fig. 2). We found that fMRI responses to INMS of single units (all except for U1; Fig
16 3. – fig supplement 1) were spatially localized within the relevant S1 digit
17 representation identified from vibrotactile stimulation. Figure 2a shows example maps
18 of digit somatotopy defined from the vibrotactile traveling-wave paradigm for
19 Participant 4 in the right and left hemispheres (left and right of the figure,
20 respectively). Figure 2b shows the BOLD response to INMS of U11 (right) and U9
21 (left) for Participant 4. These responses are well-localized within regions of the
22 somatotopic map for digit 4 of the left hand and digit 1 of the right hand, respectively.
23 Figure 2c shows the activation generated in S1 by applying vibrotactile stimulation to
24 the receptive field of U11 (right) and U9 (left). Fits to the hemodynamic responses
25 evoked in S1 by INMS and the application of vibrotactile stimulation to the unit's
26 receptive field can be seen in Figure 2d.

27 Figure 3 shows the spatial localization of the activation produced in S1 by the
28 seven perceived INMS units (U4-U6, U8-U11) (Fig. 3a) and corresponding

1 vibrotactile stimulation of each units' receptive field (Fig. 3b). In general, the BOLD
2 responses due to INMS and vibrotactile stimulation were well localized within the
3 expected digit ROI, as defined from the traveling-wave somatotopy paradigm. Figure
4 3c plots the average INMS z-score (FDR corrected) in each digit ROI, and Figure 3d
5 shows the proportion of active voxels to the INMS paradigm that were classified to
6 each digit ROI ($z > 3.08$, FDR corrected). As expected, the average z-score and
7 proportion of active voxels in the digit ROI corresponding to digits in which the INMS
8 was sensed was higher than in the neighboring digits. Figure 4 plots the group-level
9 response to show the spatial spread of the INMS and vibrotactile response to
10 neighboring digits. Figure 4a shows the mean z-score, Figure 4b the proportion of
11 active voxels and Figure 4c the GLM parameter estimate to INMS (top) and
12 vibrotactile stimulation of the unit's receptive field (bottom). ANOVA results showed a
13 significant difference in mean Z-score ($F_{4,30}=14.08$, $P < 10^{-5}$; $F_{4,30}=12.97$, $P < 10^{-5}$),
14 proportion of active voxels ($F_{4,30}=16.12$, $P < 10^{-6}$; $F_{4,30}=17.64$, $P < 10^{-6}$) and GLM
15 parameter estimates ($F_{4,30}=13.52$, $P < 10^{-5}$; $F_{4,30}=14.1$, $P < 10^{-5}$) across the stimulated
16 and neighboring digit classification (INMS; vibrotactile). A multiple pairwise
17 comparison, adjusted for multiple comparisons, showed that measures for the
18 stimulated digit were significantly higher than those of the neighboring digits for mean
19 Z-score ($P < 0.0001$ INMS; $P < 0.005$ vibrotactile stimulation), proportion of active
20 voxels ($P < 0.00005$ for INMS and vibrotactile stimulation) and GLM parameter
21 estimates ($P < 0.01$ for INMS and vibrotactile stimulation).

22 For those units lost during the fMRI run (U5, U6, U8), no areas were found to
23 show a significant loss in sensation when adding a linear parametric modulation
24 regressor to the GLM, likely due to the sudden rather than gradual loss of the unit.
25 Thus parameter estimates to INMS stimulation were not significantly different
26 between the GLM including a parametric regressor and that modelling INMS
27 stimulation alone.

28

1 **Comparison of cortical activity patterns between single unit INMS and**
2 **vibrotactile stimulation:** Participants freely described the mechanical, point-
3 vibrotactile stimulus applied to each unit's receptive field as feeling very similar in
4 extent and quality to the INMS, especially for the sensations generated from FA1
5 units. Figure 5a compares the of mapping INMS-induced fMRI responses (yellow) for
6 all FA1 single units to maps of the responses produced by applying vibrotactile
7 stimulation to the units' receptive fields (blue). Overlapping cortical responses are
8 shown in green. Activation maps show the conjunction of the individual FA1 unit
9 responses, using the same statistical threshold ($Z > 3.08$, false discovery rate (FDR)
10 correction) for both INMS and vibrotactile stimulation. BOLD responses to single unit
11 INMS were detected in a number of sensory-related brain areas, including S1, S2
12 (Brodmann areas (BA) 40 and 43), premotor cortex (PMC; SMA and dorsal PMC),
13 M1, insula (anterior insula cortex (AIC) and posterior insula cortex (PIC)), prefrontal
14 cortex (PFC) and PPC. Table 2 details the location and statistical significance (mean
15 and standard error across units) of the BOLD responses produced in these areas by
16 INMS of the five FA1 single units in the left hand. Common areas of activation for
17 INMS and vibrotactile stimulation included S1, S2, PMC, M1, and contralateral PIC;
18 however, INMS gave rise to significant activity in additional brain regions, including
19 the AIC, PPC and contralateral PFC (Table 2). Figure 5b shows that the HRFs
20 generated in these regions by INMS were similar in both onset and duration to the
21 INMS-elicited responses in S1 and S2.

22

23 **DISCUSSION**

24 The principal finding of our present work is the detailed localization in contralateral
25 S1 of cortical responses to the electrical microstimulation of single, first-order
26 mechanoreceptive afferents, and the demonstration of spatial alignment of these
27 responses with somatotopic maps derived from mechanical skin stimulation. This
28 was achieved through the combined usage of two techniques: intra-neural

1 microstimulation (INMS), to stimulate single mechanoreceptive afferents, and 7T
2 fMRI, to map the cortex with superior spatial resolution. This work also shows that
3 activity generated by stimulation of a single mechanoreceptive afferent can be
4 perceptually characterized and produces a network of cortical responses.

5 Only one previous study has combined single unit INMS with fMRI, at 3T
6 (Trulsson et al. 2001), but this was only able to resolve activation in contralateral S1
7 and S2 as the use of a surface coil limited the spatial extent of activation maps. The
8 greater signal-to-noise ratio and improved BOLD contrast afforded by 7T fMRI
9 allowed us to improve the spatial resolution, with a reduction in the voxel volume by a
10 factor of 6 compared to previous work at 3T (Trulsson et al. 2001). We have
11 exploited the improved spatial resolution to provide a detailed characterization of the
12 location and extent of the cortical network involved in encoding inputs from single
13 mechanoreceptive afferents, as well as in comparing these responses to
14 somatotopical maps created from vibrotactile skin stimulation.

15 Measurements of cortical activity elicited by INMS demonstrated that when a
16 singular, quantal touch from the stimulation of a single mechanoreceptive afferent is
17 consciously felt, a precise area in contralateral S1 is active. The response in S1 was
18 well-localized within the expected region, identified from maps of digit somatotomy
19 obtained from vibrotactile stimulation of the fingertips. The extent of the S1
20 responses to INMS was less than that elicited by vibrotactile stimulation to the unit's
21 receptive field, although the response produced by single unit INMS was relatively
22 extensive, considering that vibrotactile stimulation simultaneously engages a large
23 number of afferents (Johansson & Vallbo 1979; Vallbo & Johansson 1984).

24 Robust responses were found within the expected digital cortical area for all
25 perceived microstimulated afferents (Figs. 2 and 3), except for U1, for which no
26 significant responses were found, in either contralateral or ipsilateral S1, despite the
27 fact that the participant exhibited a complete somatotopic map of the digits in both
28 hemispheres and reported feeling the sensation throughout INMS. To explore this

1 finding further, we used the delineation of digits 2 and 3 from the somatotopic map
2 obtained with the vibrotactile traveling-wave paradigm to inspect the time series of S1
3 responses evoked by INMS for U1 (located on the palm below digit 2). We also
4 interrogated the BOLD response produced in contralateral S1 when vibrotactile
5 stimulation was applied to the receptive fields of U1. In S1, we found negative BOLD
6 responses (Fig 3. – fig supplement 1) for both INMS and vibrotactile stimulation
7 applied to the receptive field of the INMS. The negative BOLD response in this
8 subject is possibly due to a steal effect from the nearby vasculature draining from the
9 active cortex (Bianciardi et al. 2011) since draining venous regions are highly
10 modulated by block paradigms with periods of 'on' and 'off' stimulation, as used to
11 study the response to INMS and vibrotactile stimulation of the receptive field. In
12 contrast, using the traveling-wave paradigm a complete map of the digits in S1 is
13 seen. This is expected, as we have previously shown that a traveling-wave design is
14 insensitive to the non-specific BOLD contributions from large veins that drain blood
15 from across the whole hand representation in S1 (Uğurbil et al. 2003; Besle et al.
16 2013), thus suppressing the venous signal modulations found in the block
17 INMS/vibrotactile stimulation data. In order to estimate the spatial spread of INMS
18 BOLD responses to neighboring digits, we show that, at the group level, the z-score,
19 proportion of active voxels and GLM parameter estimates are significantly higher
20 ($p < 0.01$) in the stimulated ROI than in the neighboring digits (Fig. 4). These results
21 are in-line with our previous findings reported for vibrotactile stimulation (Besle 2013).

22 The network of cortical areas activated by both INMS of single
23 mechanoreceptive afferents and mechanical vibrotactile stimulation of the units'
24 receptive field, included somatosensory areas such as S1, S2, and PIC, as well as
25 areas involved in motor control, including M1, SMA and PMC. Although M1 has
26 previously been shown to be activated by tactile input (e.g. Francis et al. 2000;
27 Ackerley et al. 2012), we cannot exclude the possibility that the M1 activation
28 observed in this study may originate from spatial blurring of somatosensory activation

1 (given that M1 and S1 are located on opposite banks of the central sulcus). When
2 comparing responses to INMS and vibrotactile stimulation applied to the afferents'
3 receptive fields, INMS activated a number of additional areas, specifically the AIC,
4 PPC and PFC. Exploration of the INMS BOLD time series for these areas (Fig. 5b)
5 suggests that the activity in these areas is locked to the S1/S2 activity and is not due
6 to anticipation. Both insula and parietal cortices have been shown to contribute to the
7 perception of touch (Preusser et al. 2014), and a previous study of tactile attention
8 (Burton et al. 2008) has shown that a fronto-parietal network, which includes PFC
9 and PPC, is involved in attention. Although identical paradigm timings were used for
10 INMS and vibrotactile stimulation in order to compare the spatial localization of the
11 BOLD response, there were differences in the attentional focus between the INMS
12 and vibrotactile tasks. During the INMS fMRI runs, participants were aware that
13 perception might be lost and hence had to concentrate on the stimulus and report
14 any lack of sensation at the end of the run. In contrast, the vibrotactile stimulus was
15 delivered at a suprathreshold level and participants did not have to monitor that the
16 sensation was still present during the vibrotactile fMRI run. Hence, the increased
17 activity in AIC, PFC and PPC observed in the present study may reflect the increased
18 attentional effects (i.e., baseline or gain effects on evoked responses) during the
19 INMS protocol compared to vibrotactile stimulation. However, this is a preliminary
20 finding and requires further investigation with larger sample sizes and more
21 quantitative analysis to be corroborated.

22 The capability of combining INMS with 7T fMRI has the following theoretical
23 implications for human somatosensory research. Although the notion that peripheral
24 input from the skin is represented directly by four cytoarchitectonic areas (BA 3a, 3b,
25 1 and 2) in S1, each containing an orderly somatotopic map of the body surface has
26 been supported by findings from animal studies (Kaas et al. 1979; Paul et al. 1972;
27 Favorov et al. 1987; Tommerdahl et al. 2010) and 7T fMRI in humans (Sanchez-
28 Panchuelo et al. 2010; Sanchez-Panchuelo et al. 2012; Martuzzi et al. 2014), a

1 simple point-to-point topographical correspondence between skin surface and
2 cortical representation does not hold. In reality, there is integration and processing
3 through axonal synapsing in the dorsal column nuclei and thalamus prior to
4 mechanoreceptive information entering the cerebral cortex. There appears to be a
5 preserved transmission from single, mechanoreceptive second-order neurons in the
6 dorsal column (Vickery et al. 1994). At the level of the thalamus, an axon of a single
7 ventral posterolateral nucleus terminates over a fairly wide, roughly 0.5 mm, cortical
8 territory (Rausell & Jones 1995), where many individual thalamocortical axons
9 spread out in discrete patches over several millimeters of S1 (Landry et al. 1987).
10 This spread corresponds well with our finding that the cortical activation from a single
11 mechanoreceptive afferent extends over an area that is not dissimilar to the area
12 activated by input from many afferents through point-vibrotactile stimulation. Also,
13 neurons in S1 cortical columns have extensive lateral excitatory connections, not
14 only with neighboring neurons, but also with neurons several millimeters away in the
15 same cortical area (Burton & Fabri 1995). We have shown that single unit INMS
16 produces bilateral somatosensory activation, as well as influencing motor areas and
17 cognitive networks (e.g. PPC, PFC). Such a wide spreading of stimulus-evoked
18 activity has been clearly documented in microelectrode recording studies (Reed et al.
19 2010). Overall, the spatiotemporal pattern of S1 response to vibrotactile stimulation is
20 far from simple and its functional significance remains to be unraveled.

21 Translational insights from *in vivo* neurophysiological studies in non-human
22 primates have driven much of the theoretical understanding of cortical mechanisms
23 that govern human tactile perception, but operative procedures, especially those
24 which alter the neurochemistry of cortical synaptic transmission (Masamoto et al.
25 2009), may confound relating such findings to normal functioning of the human brain.
26 This demonstration of the feasibility of combining INMS with 7T fMRI opens up the
27 possibility of a range of further neuroimaging studies that will allow interrogation of
28 the precise anatomical and physiological properties of the fundamental encoding of

1 touch. These include systematic investigation of the sub-cortical (e.g. thalamic)
2 responses and laminar-specific cortical responses to INMS of different
3 mechanoreceptive afferent classes using a variety of electrical stimulation patterns.

4 5 **MATERIALS AND METHODS**

6 Ten experimental sessions were conducted on four right-handed participants (30-64
7 years, 2 male). Procedures were approved by the University of Nottingham Medical
8 School Ethics Committee and all participants gave full, written, informed consent.
9 Due to the precision needed in performing INMS within the magnetic resonance
10 scanner, participants were required to lie extremely still and feel relaxed; all
11 participants were accustomed to the fMRI environment (two participants had
12 participated in INMS experiments previously). Each experimental session involved
13 three steps: (1) microneurography for the characterization of a single
14 mechanoreceptive afferent (Vallbo & Hagbarth 1968); (2) assessment of the
15 sensation to INMS; (3) concurrent INMS and fMRI. Participants subsequently took
16 part in a second fMRI session in which vibrotactile stimulation was delivered.

17 Participants lay on the scanner bed with their arm (the left arm in all cases
18 except one experiment on the right arm) immobilized using cushions. Survey,
19 reference and B₀-map scans were acquired, and an image-based shimming
20 approach (Sanchez-Panchuelo et al. 2010) used to minimize magnetic field
21 inhomogeneity, with the optimized shim currents remaining fixed throughout the
22 subsequent fMRI runs. The participant was moved out of the bore of the magnet to
23 perform Steps (1) and (2).

24 **Microneurography:** In Step 1, the median nerve was accessed at the wrist in order
25 to isolate single axonal responses from mechanoreceptive afferents in the volar
26 hand, on which to perform INMS (Trulsson et al. 2001). A high-impedance (~300-500
27 kΩ), insulated, tungsten recording/stimulating electrode (15 mm length, shaft
28 diameter 0.2 mm, tip diameter ~5 μm; FHC, Bowdoin, ME) was inserted

1 percutaneously into the skin, ~3 cm from the wrist fold between the flexor carpi
2 radialis and the flexor palmaris longus tendons. An uninsulated reference electrode
3 was inserted subcutaneously 3-5 cm away, on the ulnar side of the
4 recording/stimulating electrode, and a ground electrode was attached further up the
5 participant's arm (Fig. 6). The recording/stimulating electrode was advanced into the
6 median nerve, which was located 0.3-1 cm below the skin surface. The preamplifier
7 was taped to the participant's arm, and the acquisition hardware and stimulator were
8 located at the outer edge of the scanner room (Fig. 6). Differential responses were
9 amplified (x10,000) using a preamplifier (NeuroAmpEX; ADInstruments, Castle Hill,
10 Australia), band-pass filtered (0.3-5 kHz) and sampled at 10 kHz using PowerLab
11 hardware and LabChart 7 software (ADInstruments, Castle Hill, Australia).

12 The microneurographer delivered light, stroking touch to the palm to evoke
13 activity in low-threshold mechanoreceptive afferents. A loudspeaker in the scanner
14 room allowed the microneurographer to hear the nerve activity and a projector
15 displayed the recording onto the scanner exterior for visual inspection. The
16 microneurographer systematically searched for the nerve until modulations of the
17 signal from the electrode corresponded to mass activity from mechanoreceptive
18 afferents as a result of touch were heard. Using fine adjustments, the electrode was
19 manipulated within the nerve to an intra-fascicular location and single units were
20 searched for by stroking the participant's hand.

21 Single mechanoreceptive afferents were characterized by their audio and
22 visual signals, and the extent of the receptive field of each afferent was explored
23 using a wooden stick. The location of the receptive field was mapped using von Frey
24 monofilaments and the minimal force required for mechanoreceptor activation noted.
25 Afferents were identified as being myelinated A β mechanoreceptors, namely FA1,
26 SA1, FA2 or SA2 afferents (Vallbo & Johansson 1984). The middle of the receptive
27 field was marked on the skin. Recordings of individual mechanoreceptive afferents in
28 response to mechanical stimulation were made (e.g. Fig. 1a, b) and analyzed in

1 MATLAB (The Mathworks; Natick, MA). Data were preprocessed to verify the single-
2 unit nature of all recorded mechanoreceptive afferents with an offline pattern-
3 matching algorithm.

4 **Single unit INMS:** Once a single mechanoreceptive afferent was identified, INMS
5 was carried out to ascertain the sensation produced by a low-current electrical pulse
6 sequence (Step 2). Trains of 30 Hz pulses (200 μ s, positive, square-wave pulses
7 over 0.5 s) were delivered (via Stimulus Isolator; ADInstruments, Castle Hill, Australia
8 and controlled using the LabChart 7 software). The experimenter delivered 2-3 pulse
9 sequences, while the current was increased slowly from 0 μ A, in 1 μ A steps, until the
10 participant felt a sensation. Once a clear sensation was felt, the precise location of
11 the sensation and its quality were recorded and tested to confirm whether the
12 previously mapped receptive field spatially aligned with that perceived by the
13 participant during INMS. This was done by a process of questioning the participant to
14 determine whether mechanical touch to the receptive field matched the projected
15 sensory field sensation during INMS to within \sim 1 mm. If so, it was deemed that
16 microstimulation was being applied to the afferent from which recordings had been
17 made. If the participant felt a clear small, point-sensation in the projected sensory
18 field that did not align with the mapped receptive field, the stimulated unit was
19 nevertheless explored. These units were included if the perceived sensation (e.g.
20 pressure from an SA1) was similar in quality to those in matched physiology-INMS
21 trials (e.g. perceived size, shape, sensation) (see Table 1). The stimulating current
22 intensity which generated a sensation was recorded, along with the stimulation
23 currents delivered during each fMRI run. INMS of a stable, single mechanoreceptive
24 afferent could be carried out successfully for up to \sim 45 mins, although Step 3 was
25 completed successfully for only a subset of mechanoreceptive afferents (see
26 Results).

27 **fMRI paradigm:** Each fMRI run consisted of a block paradigm, comprising 8 cycles
28 of alternating periods of 8 s INMS followed by 23 s rest (acquisition time \sim 4 mins).

1 The 8 s INMS period consisted of 0.5 s burst of stimulation (30 Hz pulse frequency;
2 200 μ s pulse width) each second. For each afferent, 1-3 fMRI repeats of the INMS
3 paradigm were conducted. In some cases, the stimulation current was adjusted
4 between runs, e.g. due to loss of perception (Vallbo et al. 1984), to ensure a clear
5 and stable sensation. If the INMS-induced sensation remained stable, other
6 parameters were also tested, including changing the stimulation frequency to 60 Hz,
7 and increasing the stimulation current to investigate the effect of recruiting further
8 mechanoreceptive afferents (Vallbo et al. 1984).

9 After Steps 1-3, fMRI of mechanical vibrotactile stimulation at each
10 microstimulated afferent's receptive field was carried out with identical timings to the
11 INMS paradigm. Vibrotactile stimuli were delivered at 30 Hz to ~ 1 mm² of the skin
12 using a piezo-electric device (Dancer Design, St-Helens, UK). In addition, the digit
13 tips of each participant's left hand (and right hand for participant 4) were stimulated
14 with 5 independently-controlled piezo-electric devices using a traveling-wave
15 paradigm (Sanchez-Panchuelo et al. 2010) to map the precise cortical representation
16 of the digits in S1. This paradigm comprised sequential vibrotactile stimulation of
17 each individual digit tip of the hand for 4 s periods of intermittent stimulation (0.1 s
18 gap every 0.5 s) at 30 Hz, over a 20 s cycle. Data were collected during two runs of
19 12 cycles each; with stimulation delivered in a forward (digit 1 to 5) and reverse order
20 (digit 5 to 1).

21 **fMRI acquisition:** MRI data were collected on a 7T scanner (Achieva; Philips,
22 Amsterdam, Netherlands) using a head volume transmit coil and 32-channel receive
23 coil (Nova Medical; Wilmington, MA). Functional data were acquired using T₂^{*}-
24 weighted, multi-slice, single-shot gradient-echo, echo-planar imaging (EPI) with echo
25 time (TE) 25 ms, repetition time (TR) 2000 ms, flip angle (FA) 75°, SENSE reduction
26 factor 3 in the right-left direction. The in-plane spatial resolution was 1.5 mm, field of
27 view of 174 \times 192 mm² in right-left and anterior-posterior directions. A slice thickness
28 of 2.5 mm was used to achieve full brain coverage (80 mm in foot-head direction)

1 within the TR period. For the traveling-wave paradigm, the slice thickness was
2 reduced to 1.5 mm (48 mm coverage) as it was only necessary to span S1.

3 Following the functional runs, a high-resolution T_2^* -weighted FLASH dataset
4 was acquired with the same slice prescription and coverage as the functional data
5 ($0.5 \times 0.5 \times 1.5 \text{ mm}^3$ resolution; TE/TR = 9.3/458 ms, FA = 32° , SENSE factor = 2) ,
6 and a whole-head structural T_1 -weighted MPRAGE dataset (1 mm isotropic
7 resolution, linear phase encoding order, TE/TR 3.7/15 ms, FA 8° , inversion time 1184
8 ms, TR-FOCI pulse (Hurley et al. 2010)) to allow projections of functional maps onto
9 flattened reconstructions of the cortical space and MNI space.

10 **fMRI data analysis:** fMRI data sets were realigned to the last volume of the data set
11 using AFNI (<http://afni.nimh.nih.gov/afni>), and statistical analysis performed using
12 mrTools (<http://www.cns.nyu.edu/heegerlab>) in MATLAB. To account for scanner drift
13 and other low-frequency signals, all time-series were high-pass filtered (0.01 Hz cut-
14 off) and data converted to percent signal change. To address the key aims, three
15 analyses were performed:

16 *Cortical responses to single unit INMS and vibrotactile stimulation in S1:* The spatial
17 localization of microstimulated afferents in S1 was compared with digit somatotopic
18 maps formed for each participant using a traveling-wave paradigm (Sanchez-
19 Panchuelo et al. 2010). The somatotopic map was used to define ROIs specific to
20 each of the 5 digits of the hand, these were subsequently used as independent ROIs
21 to allow group-level inference tests to be conducted (as performed in Besle 2013).
22 Here, data were not spatially smoothed in order to retain high spatial resolution. Both
23 the INMS data, and data acquired during vibrotactile stimulation applied to the skin
24 location where each afferent was perceived, were analyzed using a general linear
25 model (GLM) employing a canonical HRF model and its orthogonalized temporal
26 derivative. FDR adjustment (Benjamini & Hochberg 1995) was performed using an
27 adaptive step-up method (Benjamini et al. 2006). All adjusted P-values were
28 converted to quantiles of standard normal distribution (Z-score). Analysis was

1 restricted to voxels identified using the traveling-wave localizer (dilated by 5 voxels to
2 ensure complete coverage of the S1 hand area) to reduce the number of inference
3 tests on both the INMS and vibrotactile stimulation data to compute FDR corrected Z-
4 scores. We investigated the spread of INMS induced activations, and vibrotactile
5 stimulation to each unit's receptive field, by computing the mean Z-score, proportion
6 of active voxels, and GLM parameter estimates in each digit ROI. Subsequently, to
7 quantify spread of responses into neighboring digits at the group-level, INMS and
8 vibrotactile responses for the ROI corresponding to the stimulated digit were
9 combined, by averaging the mean Z-score, proportion of active voxels, and GLM
10 parameter estimates (N=7 units; 3 Digit 1 ROIs, 2 Digit 3 ROIs, 2 Digit 4 ROIs). This
11 procedure was then repeated for the 1st degree (N=11), 2nd degree (N=9), 3rd degree
12 (N=5) and 4th degree (N=3) neighboring digit ROIs. A one-way analysis of variance
13 (ANOVA) tests was then performed on this data, and post-hoc multiple pairwise
14 comparison, adjusted for multiple comparisons using Bonferroni correction.

15 For those units for which the stimulus sensation was lost during the fMRI run, a
16 further GLM analysis was run which included a regressor of linear parametric
17 modulation in time, and the associated parameter estimates were assessed.

18 Functional statistical maps from each microstimulated afferent and the traveling-wave
19 localizer were rendered onto flattened representations of the central sulcus obtained
20 using the mrFlatMesh algorithm (VISTA software, <http://white.stanford.edu/software/>)
21 based on cortical segmentations from the whole head T₁-weighted anatomical data
22 obtained using Freesurfer (<http://surfer.nmr.mgh.harvard.edu/>). Having aligned
23 functional data to the participant's whole head T₁-weighted anatomical reference
24 volume (see *Alignment of functional data*), statistical maps were transformed to
25 flattened space using linear interpolation and displayed at the central cortical depth.

26 *Whole brain analysis:* This was performed to compare those brain areas responding
27 to INMS of a single mechanoreceptive afferent with those responding to vibrotactile
28 stimulation. Data were spatially smoothed with a Gaussian FWHM 3 mm and a

1 second GLM analysis was performed on the whole volume for both the INMS data
2 and the vibrotactile stimulation data to the unit's receptive fields. The resulting Z-
3 score statistical maps were threshold at $Z < 3.08$ after FDR-adjustment and cluster-
4 correction ($p < 0.01$) to visualize activation maps and to compute binary masks for
5 each stimulated mechanoreceptive unit (and for corresponding vibrotactile
6 stimulation to each unit's receptive field).

7 Functional statistical maps from all five single FA1 afferents of the left hand
8 stimulated during INMS at 30 Hz (U1, U4, U6, U8, and U11) were projected onto
9 standard MNI space to identify active brain areas from probabilistic brain atlases
10 (Harvard-Oxford cortical structure and Talairach Daemon labels, in FSL). Functional
11 maps were transformed into the participant's whole head anatomical reference
12 volume (see *Alignment of functional data*). The whole-head anatomical T_1 -weighted
13 MPAGE from each participant was aligned to a standard T_1 -weighted MNI template
14 using first an affine FLIRT registration, followed by a FNIRT non-linear registration
15 algorithm (FSL, FNIRT). This alignment was then applied to the statistical maps from
16 the participant's INMS unit to warp the data into standard MNI space. A map was
17 computed of the intersection of responses to all five FA1 afferents, from which to
18 define significant regions of interest (ROIs). These ROIs were transformed to native
19 EPI space for each individual afferent and the beta values, Z-scores and number of
20 active voxels were interrogated for each significant ROI, in each afferent's native
21 space. Similarly, the corresponding BOLD maps resulting from vibrotactile stimulation
22 applied to the skin location where each afferent was perceived were transformed into
23 MNI space and identical analyses performed.

24 *Alignment of functional data to participant's whole head anatomical reference*
25 *volume*: Statistical maps were moved from functional acquisition space into whole-
26 head anatomical T_1 -weighted space for detailed comparison with digit somatotopy in
27 flattened reconstructions of the cortical space and for combination in standard MNI
28 space (see *Whole brain analysis*). We estimated the alignment between the

1 (distorted) reference EPI volume from the motion correction and the undistorted T_2^* -
2 weighted anatomical volume using FNIRT. Functional maps were non-linearly
3 transformed into structural T_2^* -weighted volume space using FNIRT's 'applywarp' and
4 then linearly transformed from the structural T_2^* -weighted to whole-head T_1 -weighted
5 volume space. Note that this registration was only used for the display of statistical
6 maps; all statistical analyses of functional data were performed in native EPI space.

ACKNOWLEDGEMENTS

Funding: Pain Relief Foundation grant, Medical Research Council, Vetenskapsrådet (Swedish Research Council), Royal Society International Exchanges scheme. Gratitude is extended to Professor Oleg Favorov for invaluable discussions on the manuscript.

ABBREVIATIONS

BA	Brodmann area
AIC	Anterior insular cortex
BOLD	Blood oxygenation level dependent
EPI	Echo-planar imaging
FA	Flip angle
FA1	Fast-adapting type 1 mechanoreceptive afferent
FA2	Fast-adapting type 2 mechanoreceptive afferent
FDR	False discovery rate
(f)MR(I)	(functional) magnetic resonance (imaging)
GLM	General linear model
HRF	Hemodynamic response function
INMS	Intra-neural microstimulation
M1	Primary motor cortex
PFC	Prefrontal cortex
PMC	Premotor cortex
PIC	Posterior insula cortex
PPC	Posterior parietal cortex
ROI	Region of interest
S1	Primary somatosensory cortex
S2	Secondary somatosensory cortex
SA1	Slowly-adapting type 1 mechanoreceptive afferent

SA2	Slowly-adapting type 2 mechanoreceptive afferent
SMA	Supplementary motor area
TE	Echo time
TR	Repetition time

REFERENCES

1. Paul RL, Merzenich M & Goodman H (1972) Representation of slowly and rapidly adapting cutaneous mechanoreceptors of the hand in Brodmann's areas 3 and 1 of *Macaca mulatta*. *Brain Res.* 36, 229–49.
2. Kaas J, Nelson R, Sur M, Lin C & Merzenich M (1979) Multiple representations of the body within the primary somatosensory cortex of primates. *Science* 204, 521–523.
3. Favorov OV, Diamond ME & Whitsel BL (1987) Evidence for a mosaic representation of the body surface in area 3b of the somatic cortex of cat. *Proc. Natl. Acad. Sci. U.S.A.* 84, 6606–10.
4. Penfield W & Boldrey E (1937) Somatic motor and sensory representation in the cerebral cortex of man as studied by electrical stimulation. *Brain* 60, 389–443.
5. Klatzky RL, Lederman SJ & Metzger VA (1985) Identifying objects by touch: an 'expert system'. *Percept. Psychophys.* 37, 299–302.
6. Gescheider GA, Bolanowski SJ, Pope JV & Verrillo RT (2002) A four-channel analysis of the tactile sensitivity of the fingertip: frequency selectivity, spatial summation, and temporal summation. *Somatosens. Mot. Res.* 19, 114–24.
7. Vallbo AB & Johansson RS (1984) Properties of cutaneous mechanoreceptors in the human hand related to touch sensation. *Hum. Neurobiol.* 3, 3–14.
8. Johansson R & Vallbo Å (1983) Tactile sensory coding in the glabrous skin of the human hand. *Trends Neurosci.* 6, 27–32.

9. McGlone, F et al. (2002) Functional neuroimaging studies of human somatosensory cortex. *Behav. Brain Res.* 135, 147–58.
10. Martuzzi R, van der Zwaag W, Farthouat J, Gruetter R & Blanke O (2014) Human finger somatotopy in areas 3b, 1, and 2: a 7T fMRI study using a natural stimulus. *Hum. Brain Mapp.* 35, 213–26.
11. Servos P, Lederman S, Wilson D & Gati J (2001) fMRI-derived cortical maps for haptic shape, texture, and hardness. *Brain Res. Cogn. Brain Res.* 12, 307–13.
12. Nelson AJ & Chen R (2008) Digit somatotopy within cortical areas of the postcentral gyrus in humans. *Cereb. Cortex* 18, 2341–51.
13. Sanchez-Panchuelo RM, Francis S, Bowtell R & Schluppeck D (2010) Mapping human somatosensory cortex in individual subjects with 7T functional MRI. *J. Neurophysiol.* 103, 2544–56.
14. Francis ST et al. (2000) fMRI of the responses to vibratory stimulation of digit tips. *Neuroimage* 11, 188–202.
15. Huang RS & Sereno MI (2007). Dodecapus: An MR-compatible system for somatosensory stimulation. *Neuroimage* 34, 1060–73.
16. Overduin SA & Servos P(2008) Symmetric sensorimotor somatotopy. *PLoS One* 3, e1505.
17. Blankenburg F, Ruben J, Meyer R, Schwiemann J & Villringer A (2003) Evidence for a rostral-to-caudal somatotopic organization in human primary somatosensory cortex with mirror-reversal in areas 3b and 1. *Cereb. Cortex* 13, 987–93.

18. Kampe KK, Jones RA & Auer DP (2000) Frequency dependence of the functional MRI response after electrical median nerve stimulation. *Hum. Brain Mapp.* 9, 106–14.
19. Ferretti A et al. (2007) Cortical brain responses during passive nonpainful median nerve stimulation at low frequencies (0.5-4 Hz): an fMRI study. *Hum. Brain Mapp.* 28, 645–53.
20. Vallbo AB & Hagbarth KE (1968) Activity from skin mechanoreceptors recorded percutaneously in awake human subjects. *Exp. Neurol.* 21, 270–89.
21. Torebjörk HE, Vallbo ÅB & Ochoa JL (1987) Intraneural Microstimulation in Man. *Brain* 110, 1509–1529.
22. Vallbo ÅB, Olsson KÅ, Westberg KG & Clark FJ (1984) Microstimulation of single tactile afferents from the human hand. *Brain* 107, 727–749.
23. Ochoa J & Torebjörk E (1983) Sensations evoked by intraneural microstimulation of single mechanoreceptor units innervating the human hand. *J. Physiol.* 342, 633–54.
24. Kelly E, Trulsson M & Folger S (1997) Periodic microstimulation of single mechanoreceptive afferents produces frequency-following responses in human EEG. *J. Neurophysiol.* 77, 137–144.
25. Trulsson M et al. (2001) Cortical responses to single mechanoreceptive afferent microstimulation revealed with fMRI. *Neuroimage* 13, 613–22.
26. Gelnar PA, Krauss BR, Szeverenyi NM & Apkarian AV (1998) Fingertip representation in the human somatosensory cortex: an fMRI study. *Neuroimage* 7, 261–83.

27. Sanchez-Panchuelo RM et al. (2012) Within-digit functional parcellation of Brodmann areas of the human primary somatosensory cortex using functional magnetic resonance imaging at 7Tesla. *J. Neurosci.* 32, 15815–22.
28. Gati JS, Menon RS, Ugurbil K & Rutt BK (1997) Experimental determination of the BOLD field strength dependence in vessels and tissue. *Magn. Reson. Med.* 38, 296–302.
29. Johansson RS & Vallbo AB (1979) Tactile sensibility in the human hand: relative and absolute densities of four types of mechanoreceptive units in glabrous skin. *J. Physiol.* 286, 283–300.
30. Bianciardi M, Fukunaga M, van Gelderen P, de Zwart J & Duyn J (2011) Negative BOLD-fMRI signals in large cerebral veins. *J Cereb. Blood Flow Metab.* 31, 401–12.
31. Ugurbil K, Toth L & Kim DS (2003) How accurate is magnetic resonance imaging of brain function? *Trends Neurosci.* 26, 108–14.
32. Besle J, Sánchez-Panchuelo RM, Bowtell R, Francis S & Schluppeck D (2013) Single-subject fMRI mapping at 7T of the representation of fingertips in S1: a comparison of event-related and phase-encoding designs. *J. Neurophysiol.* 109, 2293–305.
33. Ackerley R et al. (2012) An fMRI study on cortical responses during active self-touch and passive touch from others. *Front. Behav. Neurosci.* 6, 51.
34. Preusser S et al. (2014) The perception of touch and the ventral somatosensory pathway. *Brain.*

35. Burton H, Sinclair RJ & McLaren DG (2008) Cortical network for vibrotactile attention: a fMRI study. *Hum. Brain Mapp.* 29, 207–21.
36. Tommerdahl M, Favorov OV & Whitsel BL (2010) Dynamic representations of the somatosensory cortex. *Neurosci. Biobehav. Rev.* 34, 160–70.
37. Vickery RM, Gynther BD & Rowe MJ (1994) Synaptic transmission between single slowly adapting type I fibres and their cuneate target neurones in cat. *J. Physiol.* 474, 379–92.
38. Rausell E & Jones EG (1995) Extent of intracortical arborization of thalamocortical axons as a determinant of representational plasticity in monkey somatic sensory cortex. *J. Neurosci.* 15, 4270–88.
39. Landry P, Diadori P, Leclerc S & Dykes RW (1987) Morphological and electrophysiological characteristics of somatosensory thalamocortical axons studied with intra-axonal staining and recording in the cat. *Exp. brain Res.* 65, 317–30.
40. Burton H & Fabri M (1995) Ipsilateral intracortical connections of physiologically defined cutaneous representations in areas 3b and 1 of macaque monkeys: projections in the vicinity of the central sulcus. *J. Comp. Neurol.* 355, 508–38.
41. Reed JL et al. (2010) Modular processing in the hand representation of primate primary somatosensory cortex coexists with widespread activation. *J. Neurophysiol.* 104, 3136–45.
42. Masamoto K, Fukuda M, Vazquez A & Kim SG (2009) Dose-dependent effect of isoflurane on neurovascular coupling in rat cerebral cortex. *Eur. J. Neurosci.* 30, 242–50.

43. Hurley AC. (2010) Tailored RF pulse for magnetization inversion at ultrahigh field. *Magn. Reson. Med.* 63, 51–8.
44. Benjamini Y & Hochberg Y (1995) Controlling the false discovery rate: a practical and powerful approach to multiple testing. *J. R. Stat. Soc. Ser. B* 57, 289–300.
45. Benjamini Y, Krieger A & Yekutieli D (2006) Adaptive linear step-up procedures that control the false discovery rate. *Biometrika* 93, 491–507.

Figure legends

Figure 1: Physiological recordings from mechanoreceptive afferents and the location of afferents that were microstimulated during 7T fMRI.

Example microneurography recording (top) along with the instantaneous firing frequency (bottom) for (a) an FA1 afferent (U1; see Table 1) and (b) an SA1 afferent collected inside the 7T MR scanner environment. In (a), mechanical taps were delivered to the center of the FA1's receptive field and (b) a long-lasting mechanical indentation was applied at the center of the SA1's receptive field, using a wooden stick (see gray blocks). (c) Location of the afferents that were microstimulated during 7T fMRI (see Table 1). U9 was located on the right hand, but has been transposed onto the left hand for this schematic. The 'undefined' (x) afferent relates to a sensation that was felt as a line, which likely indicates two single afferents in close proximity being stimulated simultaneously.

Figure 2: Spatial localization of INMS-induced versus vibrotactile-induced responses in contralateral S1.

Activation maps related to stimulation of two different afferents in Participant 4 are rendered onto a flattened cortical patch spanning the central sulcus of the right (left of figure) and left (right of figure) hemispheres. Dark gray represents the sulci and light gray the gyri. (a) Digit somatotopy, where phase values (in radians) and corresponding preferred stimulus location (fingertip) are shown. Orderly representation of the digits is found on the posterior bank of the central sulcus (white line) and the post-central gyrus (dashed black line), corresponding to S1. (b) Statistical maps ($Z > 3.08$, FDR-adjusted) from INMS of U11 (left) and U9 (right). BOLD activation is localized within the expected digit ROI identified from digit somatotopy, as shown by the blue (digit 4) and red (digit 1) lines, which denote phase values encoded by the blue (3.77-5.03 rad) and orange (0-1.26 rad) colors respectively. The solid black line indicates the S1 hand mask (calculated by dilating

the somatotopy map by 5 voxels) within which FDR correction was performed. (c) Statistical maps ($Z > 3.08$, FDR-adjusted) for vibrotactile stimulation of the corresponding receptive fields of U11 (top) and U9 (bottom). (d) HRF estimated from the GLM analysis for INMS and vibrotactile stimulation averaged across voxels of the ROI (U10, top; U9A, bottom). Error bars show voxel-wise parameter standard errors averaged across voxels of the ROI.

Figure 3: Spread of activation across the digit ROIs identified from the somatotopy.

(a) Statistical maps ($Z > 3.08$, FDR-adjusted) from INMS of seven single units in participants 2, 3 and 4. In each case the activation map is rendered onto a flattened cortical patch spanning the central sulcus of the right hemisphere. Dark gray represents the sulci and light gray the gyri. The solid black line indicates the SI hand mask (calculated by dilating the somatotopy map by 5 voxels) within which FDR correction was performed. Activation is localized within the expected digit ROI (black line) identified from the digit somatotopy (see color legend). (b) Statistical maps ($Z > 3.08$, FDR-adjusted) for vibrotactile stimulation of the corresponding receptive field of units. (c) Z-scores (FDR-corrected) of the INMS BOLD response averaged across voxels for each of the digit ROIs identified from the traveling-wave analysis. Error bars indicate standard error across voxels in ROI. (d) Proportion of voxels activated by the INMS paradigm at $Z > 3.08$ (FDR-corrected) for each digit ROI. The source data for plots in panels (c) and (d) are available in the Figure 3 –source data 1.

Figure 4: Group analysis (N = 7 units) of the BOLD response to INMS and vibrotactile stimulation of the unit's receptive field, showing the stimulated digit compared to the neighboring digits.

(a) Z-scores (FDR-corrected) of INMS response in digit ROIs (defined from digit somatotopy) averaged across ROIs for the stimulated digit (N=7) compared to neighboring digits (1st degree neighbors, N=11; 2nd degree neighbors, N=9, 3rd

degree neighbors, $N=5$, 4th degree neighbors, $N=3$. The z-score for the stimulated digit was significantly different to that of neighboring digits. $***P<0.0001$, $**P<0.005$, statistical significance corrected for multiple comparison using Bonferroni correction

(b) Proportion of voxels activated by the INMS (top) and vibrotactile (bottom) paradigm at $Z>3.08$ (FDR-corrected) for the stimulated digit compared to the neighboring digits. Mean and standard error across ROIs. The proportion of active voxels in the stimulated digit ROI was significantly different to that of neighboring digits. $***P<0.00005$, statistical significance corrected for multiple comparison using Bonferroni procedure.

(c) GLM parameter estimates of the INMS (top) and vibrotactile (bottom) paradigm for the stimulated digit compared to the neighboring digits. The parameter estimate in the stimulated digit ROI was significantly higher than that of neighboring digits. $**P<0.01$, statistical significance corrected for multiple comparison using Bonferroni procedure. For all plots (a) – (c) the mean and standard error across N measures is shown. The source data used for the ANOVA tests are available in the Figure 4 –source data 1.

Figure 5: fMRI activation patterns and time courses in cortical areas.

(a) Cortical activation patterns in MNI space. Transverse slices and surface reconstructions showing areas of activation in response to INMS (red clusters) and mechanical vibrotactile stimulation applied directly to the respective unit's receptive field (blue clusters), as well as areas of overlap (green clusters). Clusters represent common regions of significant activation from all single FA1 units on the left hand (U1, U4, U6, U8, and U11). Individual statistical maps for each afferent were thresholded at $Z < 3.08$ after correcting for multiple comparisons (FDR) and cluster-corrected at $p = 0.01$, prior to forming the conjunction map.

(b) BOLD time courses due to INMS for U4 in different cortical areas. Responses contralateral (right) to the hand stimulation site are shown in red and ipsilateral responses are shown in blue.

Figure 6: Figure of the experimental setup.

The PowerLab, NeuroAmp EX and ML180 stimulator were placed just inside the magnet room at a field strength not exceeding 5 mT. Placement of the interface equipment within the magnet room was preferred for safety reasons, as isolated cables connected to the participant did not then pass into the control room. The USB interface and trigger cables were passed through the radio frequency shield via a waveguide aperture. An amplifier and loudspeaker was driven from the NeuroAmp EX audio output to give audio feedback to the microneurographer. In addition, a projection of the computer screen could be viewed for visual confirmation of nerve signals. A switch was used to connect the electrodes to either the stimulator or the NeuroAmp head-stage pre-amplifier. In addition, a resistive shunt was placed across the stimulation leads to remove any build-up of charge before connecting or disconnecting the stimulator. Disconnection of the stimulator was necessary because of the high level of noise introduced when it was connected. Star-quad cable was used within the magnet environment to reduce the likelihood of induced currents due to scanner operation affecting the stimulus presentation.

Tables

Table 1: mechanoreceptive afferent units in which INMS was performed during 7T fMRI.

The table details the unit type and location, as well as the frequency and perception of applied INMS. All units were located on the left hand unless stated.

*A small line sensation is indicative of the simultaneous stimulation of two afferents that are in close proximity.

Participant	Unit	Type	Location	Physiology	Sensation	Frequency
1	1A	FA1	Palm	Yes	Buzzing	30 Hz
2	2	FA1	Base of digit 1	Yes	Small dots	60 Hz
	3	SA1	Middle of digit 1	Yes	Pulling	30 Hz
	4	SA1	Base of digit 1	Yes	Pulling	30 Hz 60 Hz
	5	FA1	Middle of digit 1	Yes	Vibration	60 Hz
	6A	FA1	Digit 3 fingertip	No	Tapping, vibration	30 Hz 60 Hz 90 Hz
3	7	FA1	Base of digit 3	Yes	Small, round point of tingle sensation	30 Hz
	8A	FA1	Digit 3 fingertip	No	Small, round point of tingle sensation	30 Hz 60 Hz 90 Hz
4	9A	FA1	Middle of digit 1 (<i>right hand</i>)	No	Prickle, flutter	30 Hz
	10	Undefined	Digit 4 fingertip	No	Small line*	30 Hz
	11A	FA1	Middle of digit 4	No	Flutter	30 Hz

Table 2: Cortical areas showing significant activation to INMS of single mechanoreceptive afferents and the corresponding vibrotactile stimulation.

Results show the mean and standard error across the five FA1 mechanoreceptive afferents subject to INMS at 30 Hz and corresponding vibrotactile stimulation of the perceived sensation, showing the number of units showing significant activation, MNI coordinates, beta values, Z-score and number of voxels in ROI. Source files for Table 2- source data 1 and Table-2 source data 2 contain single unit INMS and vibrotactile stimulation results, respectively, for each of the 5 (U1, U4, U6, U8, U11) individual units.

ROI	No. Units	x, y, z MNI co-ordinates	Single unit INMS			Vibrotactile stimulation		
			Beta	Z	Voxels	Beta	Z	Voxels
SI R	4	54, -12, 46	1.4±0.2	5.9±0.5	38±7	1.3±0.3	5.4±0.3	41±12
SI L	3	-52, -12, 44	1.2±0.2	5.6±0.8	20±9	1.6±0.3	5.2±0.2	19±1
BA 40 R	5	60, -22, 16	1.4±0.2	4.9±0.2	56±5	1.4±0.1	4.8±0.2	54±7
BA 40 L	4	-60, -22, 16	1.5±0.4	5.3±0.2	73±5	1.4±0.2	5.0±0.1	72±12
BA 43 R	2	60, -4, 10	1.1±0.4	5.4±0.1	45±6	1.2±0.4	4.4±0.2	30±20
BA 43 L	3	-58, -12, 14	1.0±0.4	4.8±0.3	33±8	1.7±0.3	4.2±0.2	26±11
SMA R	5	4, 0, 60	1.2±0.2	4.8±0.3	93±27	1.3±0.2	4.8±0.2	43±21
SMA L	5	-2, 0, 60	1.2±0.2	4.5±0.3	66±19	1.2±0.1	4.5±0.3	29±6
PMC R	4	54, 0, 50	0.8±0.2	4.7±0.2	36±11	1.1±0.2	5.0±0.2	46±9
PMC L	5	-52, -2, 50	1.1±0.1	5.5±0.3	37±7	1.2±0.1	4.3±0.1	20±8
M1 R	3	54, -6, 48	0.9±0.2	5.2±0.5	51±20	0.8±0.2	5.0±0.7	31±10
M1 L	2	-52, -6, 48	1.5±0.2	6.3±0.1	66±36	1.3±0.1	5.3±0.5	21±3
PIC R	5	46, -2, 10	0.8±0.2	4.2±0.2	45±12	0.8±0.2	4.7±0.2	27±3
PIC L	5	-42, -2, 10	0.8±0.1	4.4±0.2	38±14	-	-	-
AIC R	4	34, 26, 4	1.2±0.1	4.7±0.2	146±20	-	-	-
AIC L	4	-32, 26, 4	1.1±0.1	4.4±0.2	106±21	-	-	-
PPC R	4	38, -48, 50	1.2±0.1	4.4±0.3	168±44	-	-	-
PPC L	5	-38, -48, 56	1.0±0.1	4.4±0.3	172±43	-	-	-
PFC R	4	42, 34, 18	1.2±0.2	4.5±0.3	78±22	-	-	-

Figure Supplements

Figure 3- figure supplement 1.

Comparison of contralateral S1 responses to different paradigms for Participant 1.

Statistical maps overlaid on a high resolution T_2^* -weighted structural image. (a) Digit somatotopic maps obtained with the traveling-wave paradigm for both hands, showing the location of the maps in the posterior bank of the central sulcus. (b) Map of veins identified using T_2^* -weighted magnitude and phase images. Phase images are unwrapped and high-pass filtered. A map of veins is approximated by thresholding the unwrapped, filtered phase image and convolving the identified voxels with a 2 mm kernel. (c) Statistical maps ($Z > 3.08$, FDR-adjusted) for INMS of U1. Note, there is no activation in the S1 hand area, as shown by the ROIs delineating each of the digits. (d) Time series of the BOLD response to INMS of U1 for the digit 2 ROI, denoted by the green line in image (upper panel) and of a region of activation co-localized with a vein as indicated by the white circle (lower panel).

Source data

Table 2- source data 1.

Source files for single unit INMS.

This matlab file contains 2D-matrices (19x5) with the results for single unit INMS for each of the 5 individual units (U1, U4, U6, U8, U11) in each of the 19 ROIs. 'BetaValues' contains mean across voxels of the beta values, 'Z-score' contains the mean Z_score (FDR- corrected) across voxels and 'NumberVoxels' contains the number of significant active voxels ($Z > 3.08$, FDR-corrected) in the ROI. Table 2 summarizes the results by showing the mean and standard error across the 5 units.

Table 2- source data 2.

Source files for vibrotactile stimulation.

This matlab file contains 2D-matrices (19 ROIs x 5 units) with the results for vibrotactile stimulation applied to the receptive field for each of the 5 individual units (U1, U4, U6, U8, U11) in each ROI. 'BetaValues' contains mean across voxels of the beta values, 'Z_score' contains the mean Z-score (FDR- corrected) across voxels and 'NumberVoxels' contains the number of significant active voxels ($Z > 3.08$, FDR-corrected) in the ROI. Table 2 summarizes the results by showing the mean and standard error across the 5 units.

Figure 3- source data 1.

Source files for plots of Z-score and Proportion of active voxels in each Digit ROI.

This matlab file contains variables for each individual unit (U4, U5, U6, U8, U9, U11) with fields 'micro_stats' and 'vibro_stats' containing a structure with the results for single unit INMS and vibrotactile stimulation of the unit's receptive field, respectively. Each structure has the following fields: 'zetaMean', 'betaSem': (5 digits x 1)-vector

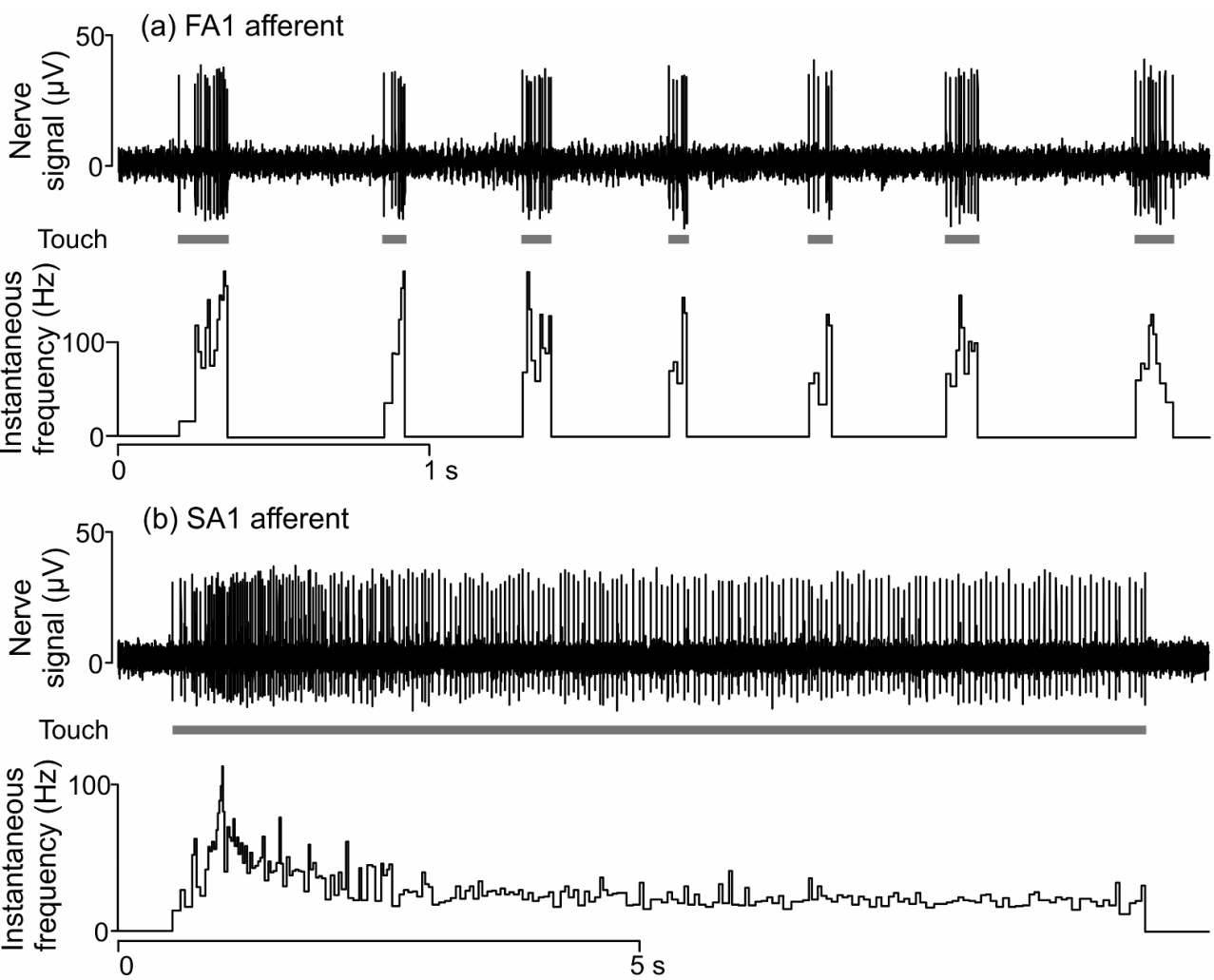
containing mean Z-score (FDR-corrected) and standard error across voxels for each Digit ROI; 'PropActVox': (5 digits x 1)-vector containing proportion of active voxels ($Z > 3.08$, FDR-corrected) in each Digit ROI; and 'betaMean', 'betaSem': (5 digits x 1)-vector containing mean GLM parameter estimate and standard error across voxels for each Digit ROI. GLM parameter estimates are not plot in Figure 3 but are used for subsequent group analysis.

Figure 4- source data 1.

Source files for ANOVA tests.

This matlab file contains the 2D-matrices (11 x 5), related to each panel in Figure 4, that were used for the 1-way analysis of variance (performed using the 'anova1' matlab command). Each matrix row contains data for each of the 7 units (there are up to eleven 1st degree neighboring digit ROIs) and each matrix columns represents the 'proximity' to the stimulated digit ROI (stimulated digit ROI, 1st degree, 2nd degree, 3rd degree and 4th degree neighboring digit ROIs). 'Zeta_micro' and 'Zeta_vibro' are the matrices containing the Z-score (FDR-corrected) values, 'PerVox_micro' and 'PerVox_vibro' contain the proportion of active voxels ($Z > 3.08$, FDR-corrected) and 'Beta_micro' and 'Beta_vibro' contain the GLM parameter estimates for INMS and vibrotactile stimulation respectively. ANOVA results show a significant difference in mean Z-score ($F_{4,30}=14.08$, $P < 10^{-5}$; $F_{4,30}=12.97$, $P < 10^{-5}$), proportion of active voxels ($F_{4,30}=16.12$, $P < 10^{-6}$; $F_{4,30}=17.64$, $P < 10^{-6}$) and GLM parameter estimates ($F_{4,30}=13.52$, $P < 10^{-5}$; $F_{4,30}=14.1$, $P < 10^{-5}$) across the stimulated and neighboring digit classification (INMS; vibrotactile).

Figure 1



(c) Units microstimulated during concurrent UHF fMRI

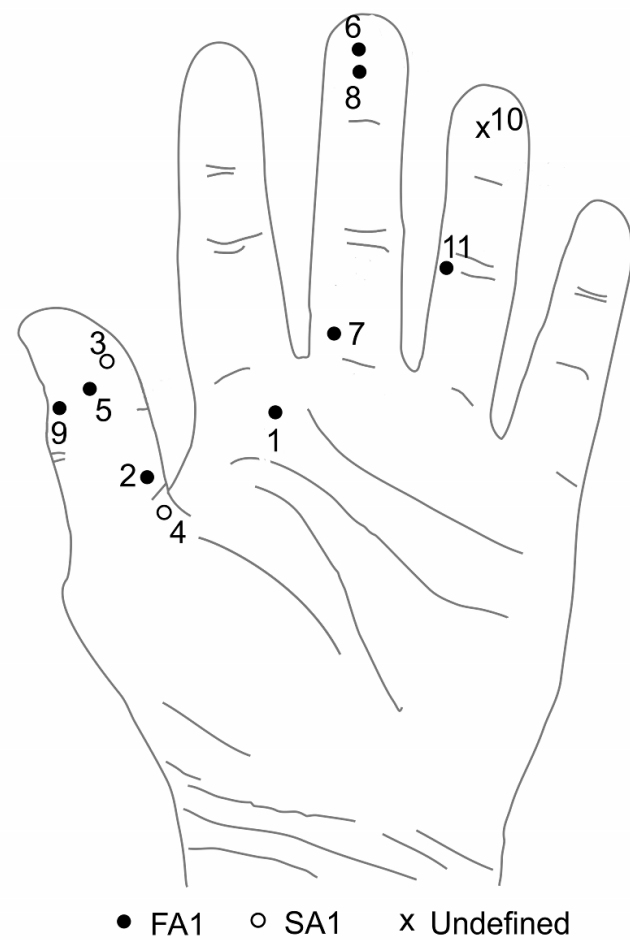


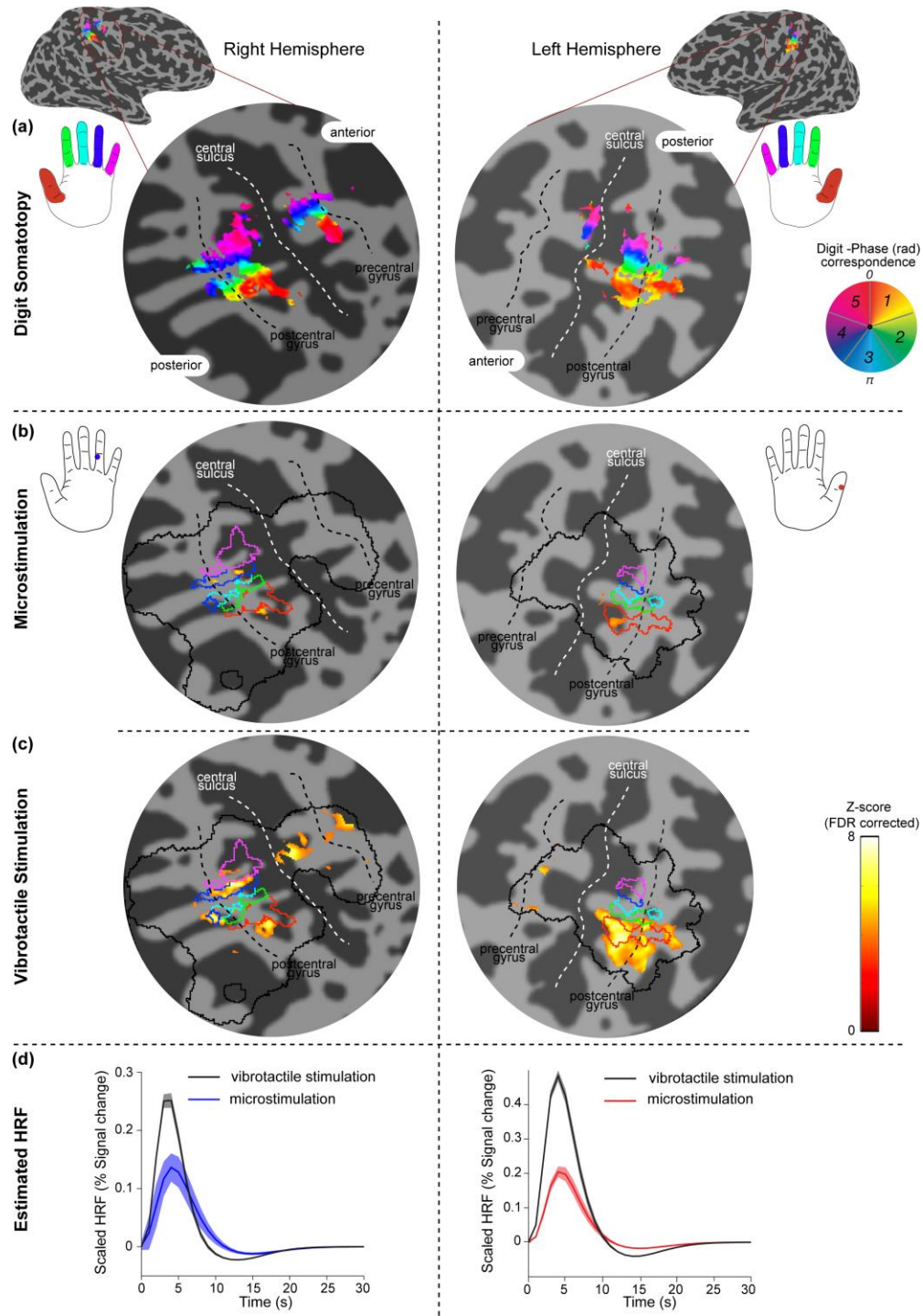
Figure 2

Figure 4

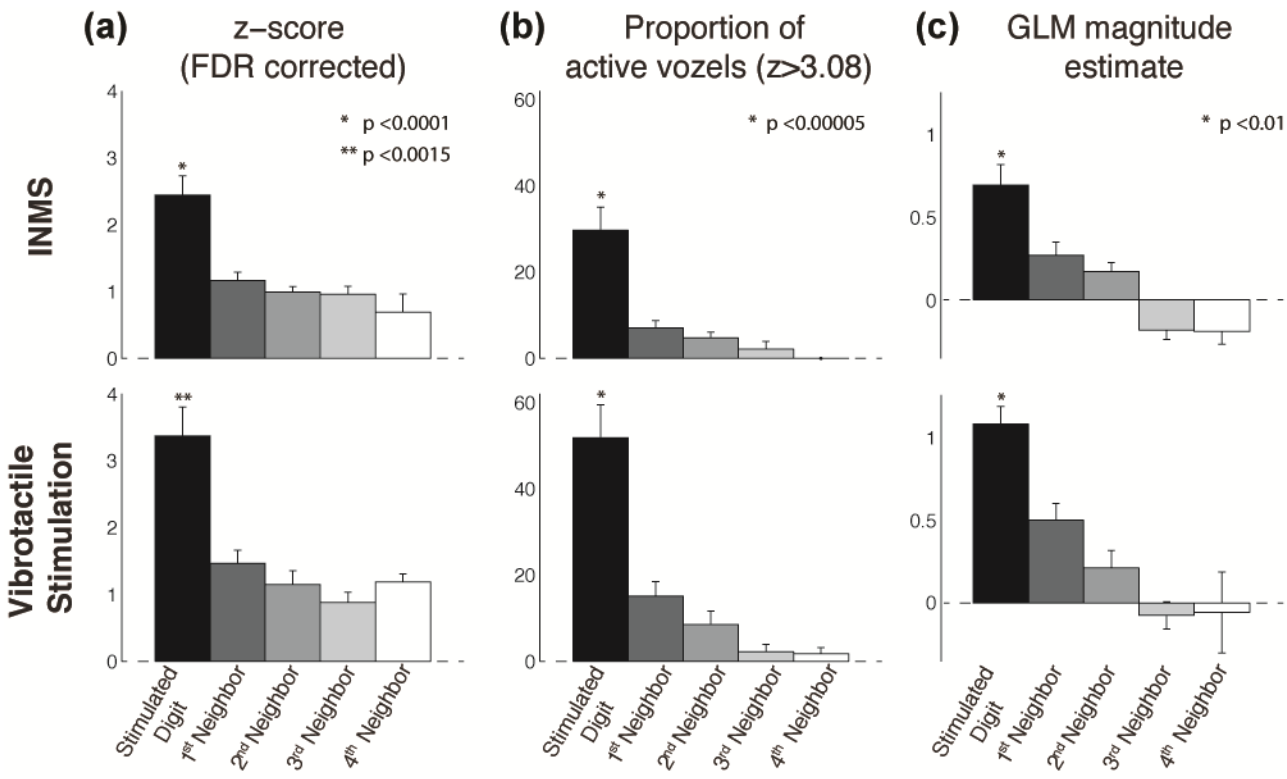


Figure 5

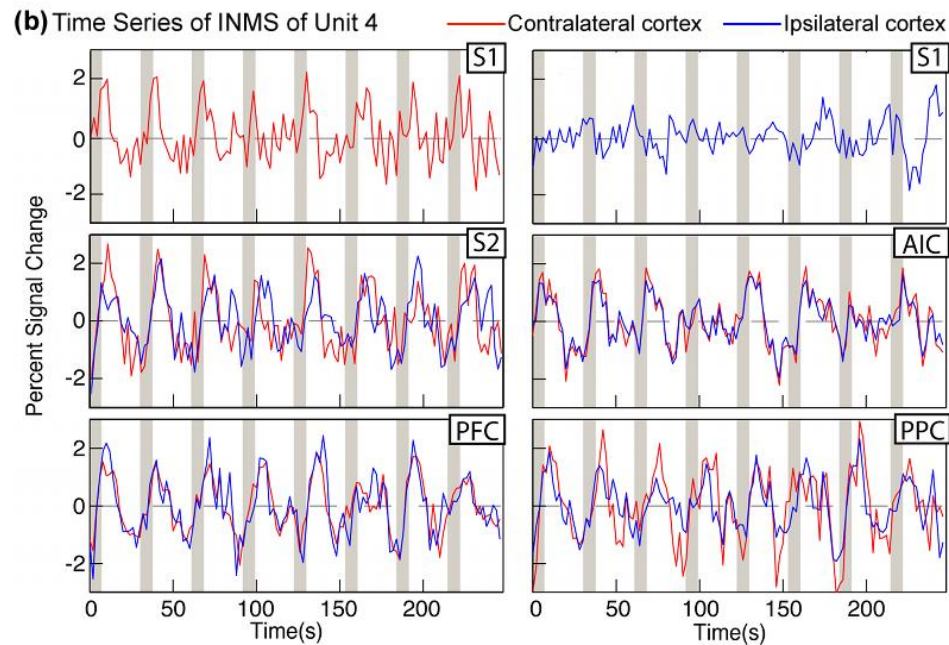
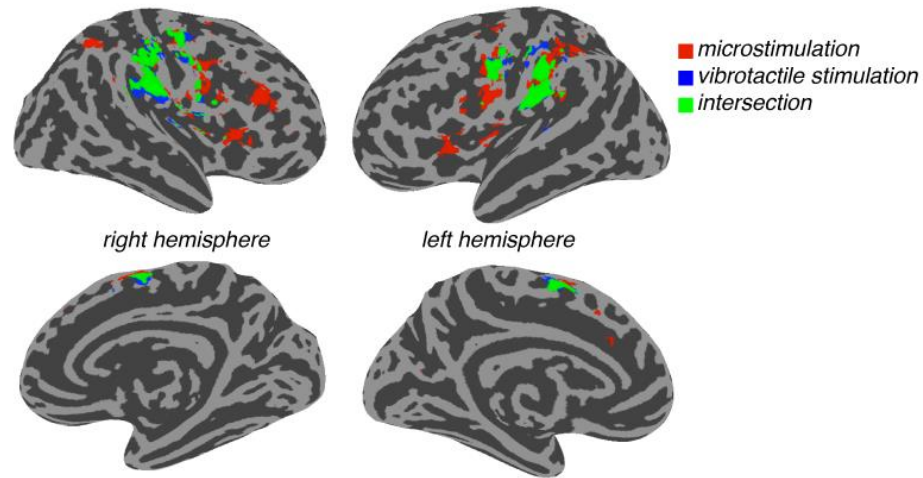
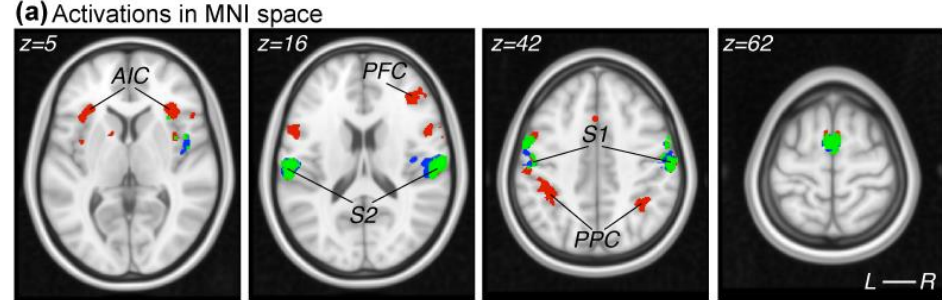
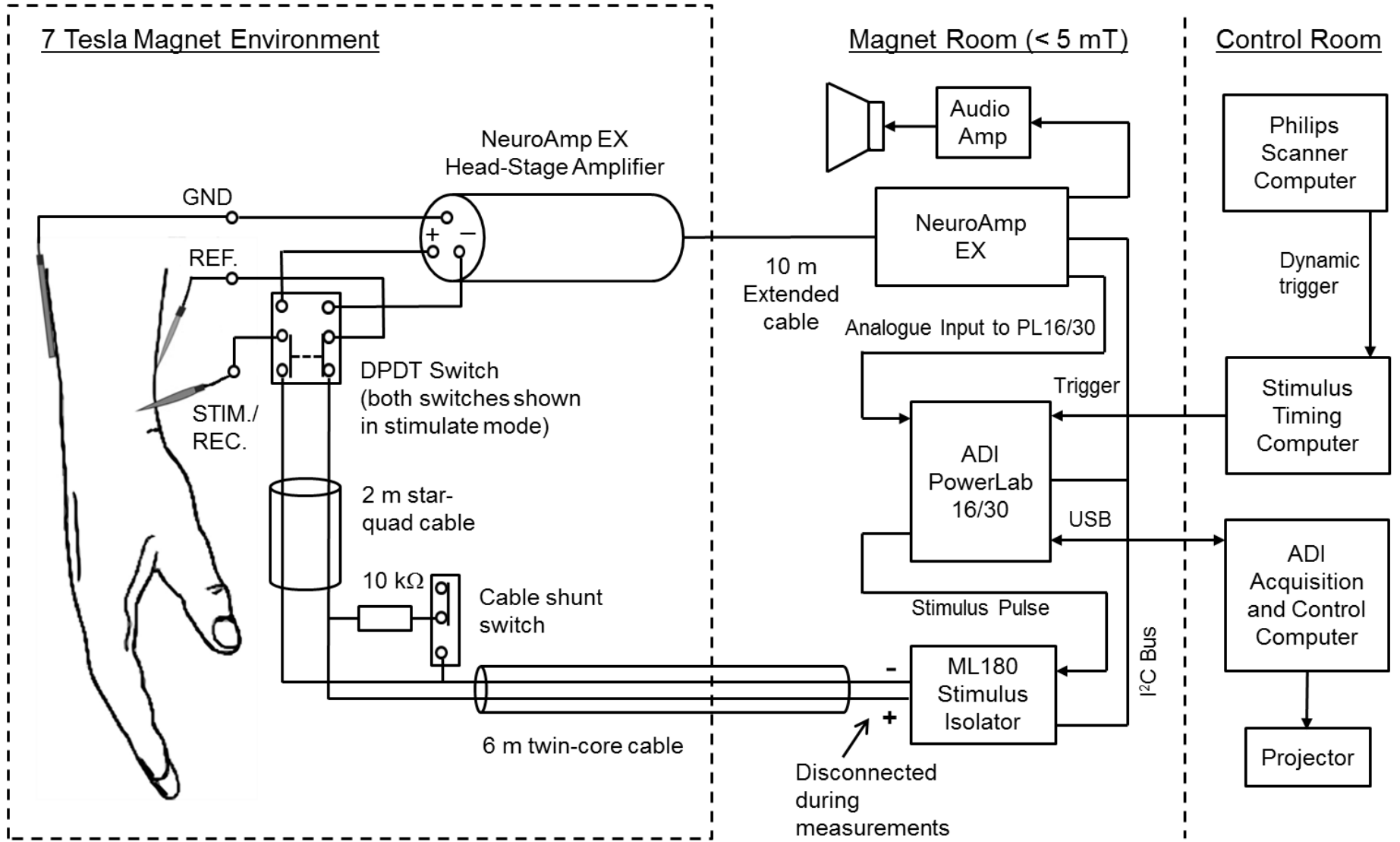
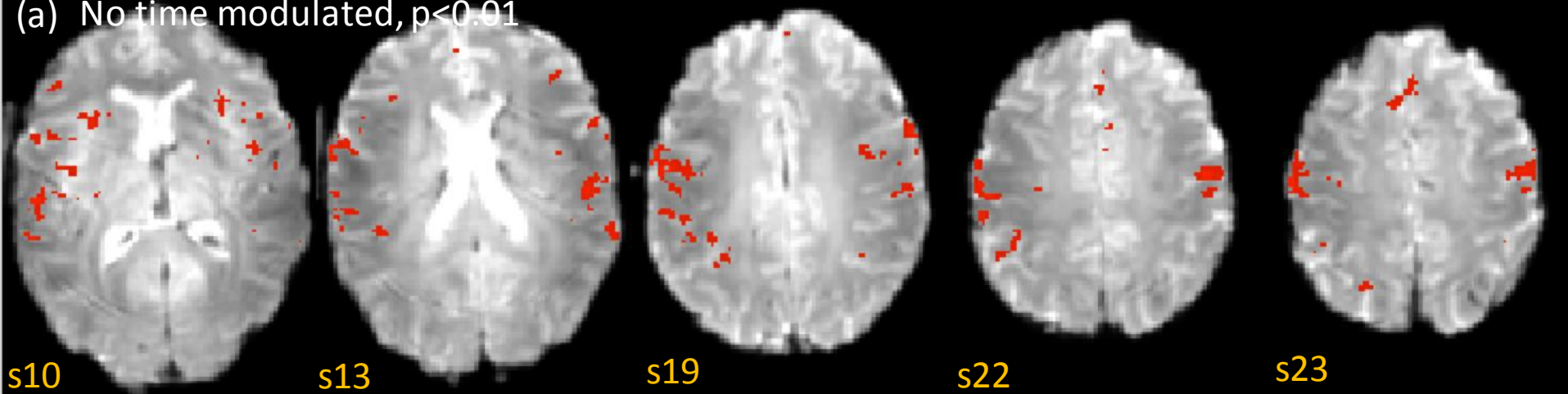


Figure 6

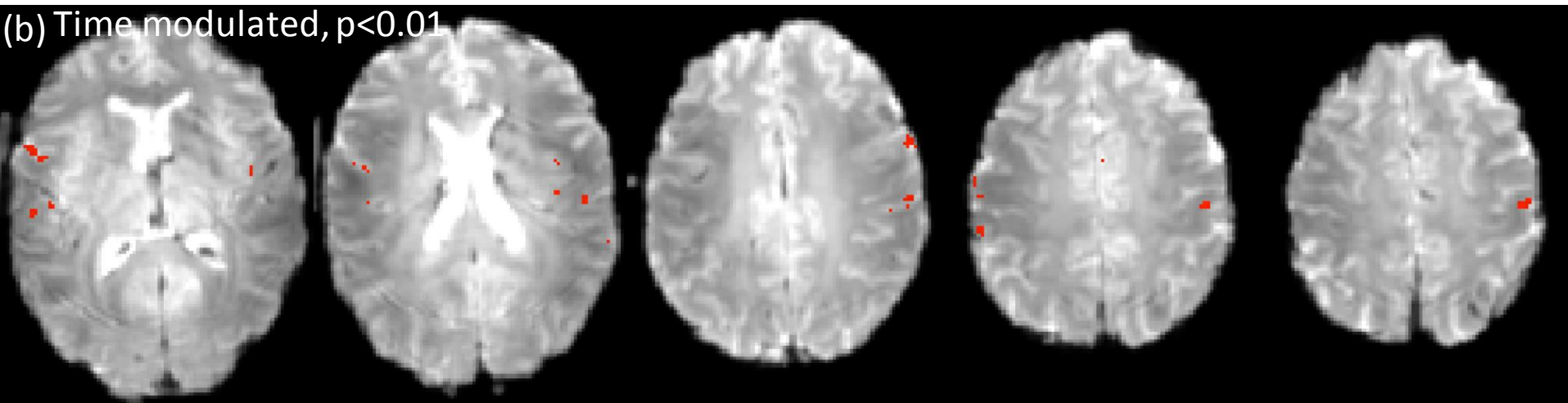


Parametric Modulation for Reviewers

(a) No time modulated, $p < 0.01$



(b) Time modulated, $p < 0.01$



Beta values across active voxels ($p < 0.01 \sim T = 2.35$):

No time modulated: $\beta = 1.02$ (0.04 sem)

Time modulated: $\beta_1 = 1.05$ (0.04 sem)

$\beta_2 = -0.35$ (0.01 sem)

